Control of work function of indium tin oxide: a surface treatment by atmospheric-pressure plasma layer on fabric-type electrodes

Yoshihiko Ueda[1]*, Junichi Abe[2], Hideyuki Murata[2], Yasuhito Gotoh[1], and Osamu Sakai[1]

[1]*Department of Electronic Science and Engineering, Kyoto University, Kyoto-daigaku Katsura, Nishikyo-ku, Kyoto 615-8510, Japan*

[2]*School of Materials Science, Japan Advanced Institute of Science and Technology, 1-1 Asahidai, Nomi, Ishikawa 923-1292, Japan*

The surface electronic properties of metal oxides, which affect the performances of layered electronic devices, are controlled by non-thermal atmospheric-pressure plasmas generated using a fabric-type electrode and gas flow induced through this plasma layer. We specify a method to control the work function of indium tin oxide (ITO) films by this plasma, in which such reactive species as oxidant radicals are generated. These oxidants are spatially transported in the gas flow to the ITO surface and increase the ITO's work function, as verified in our experimental results. To examine the effects of the increased work function in a specific electronic device, we treat the surface of an ITO electrode in an organic light-emitting diode and observe the enhancement of the light-emitting efficiency.

1. Introduction

The electronic properties on the surfaces of solid-state materials[1)] play significant roles when the surfaces contact other layers that are composed of different materials and form junctions. The bulk properties in the layers are also important, but the surface properties, one of which is the work function, are often more crucial. For instance, organic light-emitting diodes (OLEDs) are one multi-layered electronic device, and efficient injections of electrons and holes through the junctions between the layers into the light emitting layer increase their light-emitting efficiency and lower the operation voltage.[2)] To control the electronic properties on the surfaces, such methods as removing the impure molecules attached on the surfaces and inserting a thin-film buffer layer have been used in the industrial fabrication processes of electronic devices.

In this report, we examine the control of the work function and how it is performed by atmospheric-pressure plasmas. Recently, many atmospheric-pressure plasmas have

*E-mail address: yoshi-calling.1090bz@cool.zaq.jp

been studied for industrial applications in various treatments of solids, biomaterials, and liquids. We reported several schemes, in which novel electrode configurations led to various chemical reactions that are effective on material processing.[3–8] In our previous report,[5] we proposed a fabric-type electrode as an active filter in flowing fluids, such as gases and liquids. A fabric-type electrode has a two-dimensional plane structure around which atmospheric-pressure plasmas are generated. Since this plane structure has "holes" or "vacancies" that are occupied by plasmas and fluids that can penetrate them, the fluids are reformed and involve active species like radicals and short-lifetime intermediates. Such filter-like functions of various atmospheric-pressure (micro)plasma layers have been proposed for material synthesis.[9–13] We set indium tin oxide (ITO) thin films in the downstream region of the gas flow and observed the increase of the work function,[5] in which OH or other radicals are key species for its increase. However, we neither examined the details of the parameter dependences nor investigated the effects of the work function enhancement for applications of electronic devices.

Following those results, in this report, we address the control of the work function of metal oxides including ITO and Ga-doped ZnO (GZO) with this filter-like atmospheric-pressure plasma. We demonstrate the rapid enhancement of the work functions of ITO and GZO using this method and apply it to the surface treatment of ITO electrodes in OLEDs. We also perform diagnostics of gaseous phases and study possible reactions and the spatial transport of generated oxidants, such as OH and O_3.

2. Experimental setup

We used a similar experimental setup for the treatment of the flat surfaces of metal oxides,[4,5] and the total schematic view of our experimental apparatus is shown in Fig. 1. Plasmas were generated on a "fabric-type" electrode that had a plane fabric structure with a filter-like structure. Inlet gases flowed between the wire electrodes with 1.0-mm separation both in the lateral and horizontal directions; 200-μm diameter Cu wires were covered by a 180-μm thick teflon layer, enabling us to obtain two-dimensional atmospheric-air plasmas at ignition voltage less than 2 kV, localized on the electrode surfaces within a 1-mm distance.[4] We used Ar at 2 L/min with a H_2O bubbling setup in which the temperature was kept at room temperature (300 K), and Ar bubbles were injected from a 1/4-inch tube and floated up 5 cm through the water. In cases without water vapor, the Ar gas flow did not pass through the water bubbling process in the H_2O container, as shown in the double dotted lines. On the other hand, the

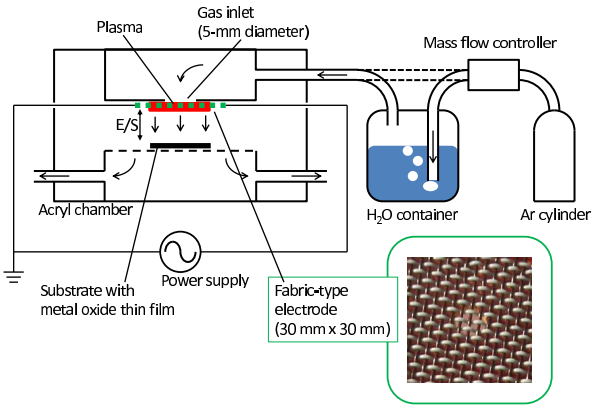

Fig. 1. Schematic view of experimental apparatus to control work functions of ITO and GZO. Distance between electrode and substrate (E/S) is 3.5 mm.

Ar gas flow did pass through the H_2O container in cases with water vapor, whose partial pressure was in the similar range of saturated H_2O vapor pressure ($\sim$ 4%). The amplitude of the discharge voltage was 1.8 kV_{0p} in the sinusoidal waveform at 13.4 kHz, and the target material faced this gas flow after the laminar plasma layer. Since plasmas were generated in the dielectric barrier discharges, the increase of the gas temperature was limited by 130 degrees or less; our previous study[3)] on similar dielectric barrier discharges indicated that the highest gas temperature was around 400 K in the atmospheric-pressure discharge with a thickness of 0.5-1.0 mm. We did not control the temperature during any part of the setup during the surface treatment, and the temperature of the treated materials remained around 300 K in the gas flow.

The treatment materials were set apart from the plasma layer by 3.5 mm (distance between electrode and substrate, E/S). Since the lifetime of the electrons in the atmospheric-pressure plasmas is 1 μs or less[14)] and the plasmas cannot be attached to the materials' surfaces, this is a remote plasma treatment system. The materials for the work-function enhancement were ITO and 10-wt% Ga-doped ZnO (GZO) films with thicknesses of 300-500 nm deposited on 10 $\times$ 10 mm^2 glass substrates by a radio frequency magnetron sputtering method. These two thin metal-oxide films had a sheet resistance around 10 Ω/sq.

After the treatment, we measured the work functions with the Kelvin probe method (MacAllister, KP6500) and used a vacuum-deposited Au film as a standard sample to determine their absolute values from the acquired data.[15,16)] The measurement results of

the work functions were compared with the ionization potentials monitored by photoemission yield spectroscopy (Riken Keiki, AC-2) and performed within two hours after the treatments were finished, except for the measurement of the long-term variation shown in Fig. 4.

Furthermore, we applied this scheme to improve the characteristics of the organic light-emitting diodes (OLEDs) by changing the surface states on the ITO electrodes as follows. We used the treatment of the ITO electrodes for the hole transport in the OLEDs and observed the changes of the emission efficiency after a few treatments of the ITO surfaces that included this scheme. So far, we have investigated several effects that improved the interfacial characteristics of the OLEDs.[2,21] We fabricated a bilayer OLED using *N*,*N*-di(naphthalen-1-yl)-*N*,*N*'-diphenyl-benzidine (α-NPD) as a hole-transport layer and tris(8-hydroxyquinoline)aluminum (Alq_3) as an emitting electron-transport layer. On the Alq_3 layer, Al was deposited for the electrode, and a thin LiF layer was inserted between the Alq_3 and Al layers.[2] All the fabrication procedures resembled those in Ref.[2] except the process described below. The ITO electrode, which was the main target of the surface treatment described here, was located beneath the α-NPD layer. The highest occupied molecular orbital of α-NPD (HOMO, > 5 eV) is higher than the work function of ITO (~ 4.8 eV in this study); this gap is an obstacle against the transport of holes, and excessive external voltage is required to overcome it. One way to reduce this obstacle is to use ultra-violet (UV) ray irradiation and O_3 flux on the ITO surface;[17] UV rays activate the ITO surface to form an O-rich thin layer during the O_3 flux. Here, we applied the Ar plasma treatment of the ITO surface.

To investigate the gaseous phases in the plasmas and the downstream regions of the plasmas above the treatment surfaces, we performed optical emission spectroscopy (OES) using a spectrometer (USB2000, Ocean Optics). The optical fiber's inlet, which guided the light to the spectrometer, was set at the substrate position. During the OES measurements, the substrate was replaced by the quartz glass behind which the fiber inlet was fixed. In the 1-mm downstream region on the discharge electrode, we also performed O_3 absorption spectroscopy in the ultra-violet ray range using a commercially available Hg lamp and a spectrometer.

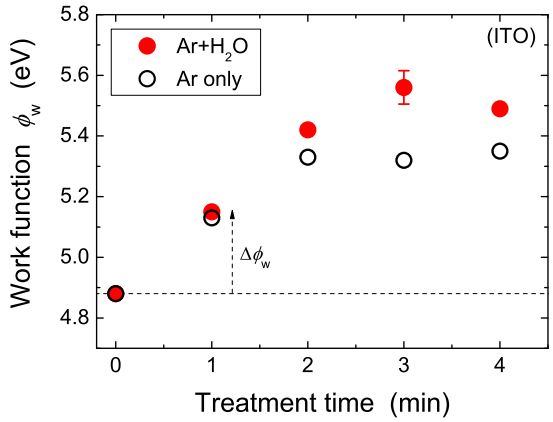

Fig. 2. Change of work function of ITO films as a function of treatment time downstream of atmospheric-pressure plasmas with and without water vapor. Horizontal dotted line indicates initial value of ϕ_w before treatment.

3. Experimental results and discussion

3.1 Surface treatments of metal oxides

Figure 2 shows the treatment time dependence of the work function of the ITO films measured two hours after the treatment. We plotted a typical error bar shown at three minutes; throughout the work function measurements, the acquired data included similar errors. The work function increased rapidly within two minutes of the treatment and became saturated. The addition of H_2O vapor through the bubbling process (Ar + H_2O) enhanced this increase. Such a rapid increase of the work function on surfaces with localized areas in the atmospheric-pressure dry processes has not been reported so far, although our previous report indicated the treatment's localized effect.[5)]

The ionization potential, shown in Fig. 3, increased in a similar manner with a similar increase rate, confirming that clear changes took place on the surfaces of the ITO films. These two results (Figs. 2 and 3) indicate significant modification of the surface electronic states in this scheme. In addition, since the ionization potential resembled the work function, this scheme is at least effective on degenerated electronic materials in which the Fermi level is in the conduction band. The difference of these two results between the work function and ionization potential measurements was found around one minute, where the ionization potential increased more rapidly. We cannot precisely point out why such a difference occurred, but a certain distribution range of the electronic states in the energy levels might make the threshold energy of the flow-

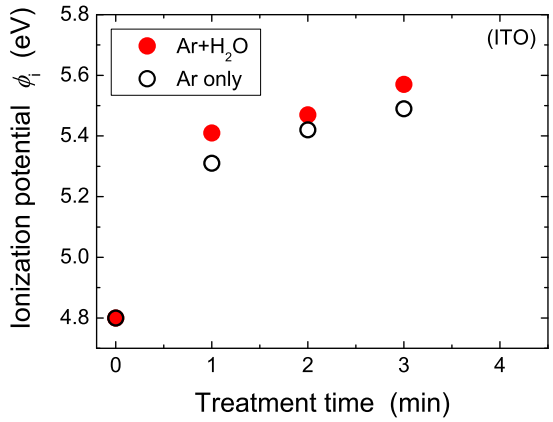

Fig. 3. Change of ionization potential of ITO films as a function of treatment time downstream of atmospheric-pressure plasmas

ing photoionization current uncertain. That is, in the photoemission yield spectroscopy, the threshold photo energy in the optical response with varying wavelengths defines the ionization potential, but the threshold value is very sensitive to local perturbations of the energy band edge, which is sometimes slightly vague. On the other hand, the work function monitored by the Kelvin probe is defined as spatially averaged electric potential.

In cases of work function control by other methods, such as O_3 supply after ultraviolet ray irradiation,[17] long-term variation causes a problem, because increased work function usually returns to its initial value within several hours after the treatment. However, in this method described here, the enhancement of the work function was effective for the time range of the days of the storage. Figure 4 shows the variation of the increased work function of the treated sample with H_2O vapor, where we measured the work function twice: two and 240 hours after using the same samples. This result indicates that the work function enhancement remained for ten days after the treatment even if we stored the films in a customary low-humidity air-filled container.

To further confirm the validity of this method to control surface electronic states by atmospheric-pressure plasmas, we used GZO films and performed a similar treatment. Fig. 5 shows the GZO cases that closely resemble those in Fig. 2; the increased value and the enhancement rate of the work function is in the same range. This method's validity is not limited to ITO but is also applicable to GZO cases whose surface electronic properties are dependent on the surface distribution of O-rich layers.

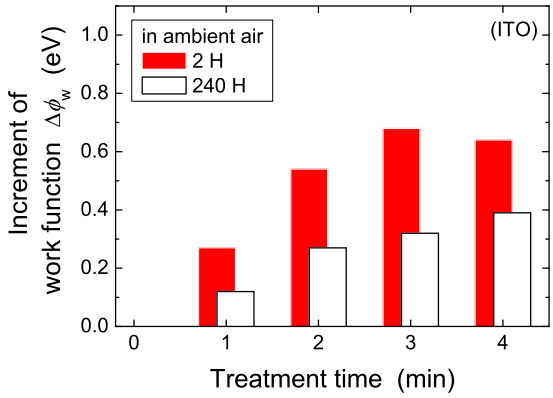

Fig. 4. Long-term variation of increased work function of ITO films as function of treatment time in downstream of atmospheric-pressure plasmas. For films with 240-hour storage after treatment, we stored them in air-filled containers with low humidity.

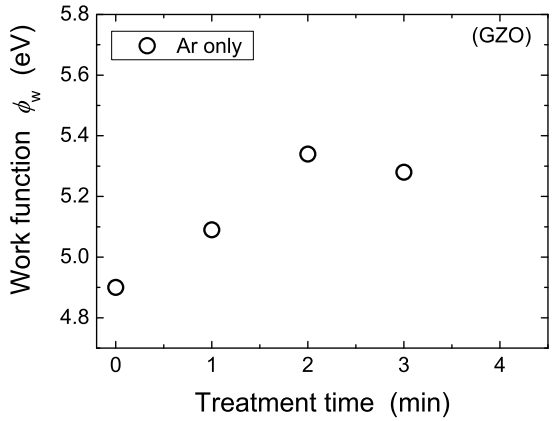

Fig. 5. Change of work function of GZO films as a function of treatment time downstream of atmospheric-pressure plasmas

So far, we have examined the macroscopic properties of the surfaces, which arise in the total effect(s) from microscopic states like various surface bonds. To obtain surface information in a microscopic view, we performed X-ray photoelectron spectroscopy (XPS) without using the ion bombardment treatment that is sometimes applied before surface observation since it might remove significant surface information. Figure 6 shows the entire and enlarged views of the spectra, and we can see the In and Sn signals as usual in ITO films. One apparent change after the plasma treatments is the reduction

of the C signal in both cases with and without water vapor, producing surface cleaning effects by species generated in the layer of the atmospheric-pressure plasmas.

Another change observed in Fig. 6 is the intensity of O 1s. The data obtained from 528 to 535 eV include two O-oriented states (O^{2-} and OH), and the spectra are usually convoluted. In the case without water vapor, the spectrum around 530.5 eV became large, which indicates an increase of O^{2-} density on and/or near the surface.[18] On the other hand, in the case with water vapor, the spectrum around 532.0 eV became large, which indicates an increase of the OH group.[18] This observation is summarized as follows: (i) The OH group on a solid surface usually increases its work function by the surface layer of electric dipole moments, and (ii) O-rich layers also increase the work function. In both cases, when oxygens are incorporated into the ITO structure near the surface or on its surface through the unsaturated dangling bonds that remain in as-grown ITO, the incorporated positions are charged negatively. Then the oxygens repel the free electrons in the conduction band, increasing the work function.[17] These two facts (i) and (ii) support the experimental observations that increase the work function, and the OH effect is larger than that of O^{2-} on the increases in our experiment.

Comparing the results with others in the previous reports that show the cases in low-pressure and atmospheric-pressure plasma treatments,[17,19,20] the process parameters on the required time and the increment factor were favorably improved. Although the mechanism cannot be described clearly, a decrease of the C concentration leads to an increase of the work function. However, we cannot explain the changes of the work function in our experiment by the change of the C concentration. Compared with previous studies,[17,20] the decreasing rate of the C concentration is similar, but the increased work function (more than 0.6 eV at maximum) is higher than those in previous reports (0.3-0.5 eV). This difference is attributed to changes of the O 1s spectra. The differences from previous studies indicate that our method using the atmospheric pressure process in remote plasma treatment supplies more oxidants due to higher electron density ($10^{12} - 10^{13}\mathrm{cm}^{-3}$),[4] and the transported oxidants work in the equilibrium state of the surface chemisorption and/or stable physisorption. As indicated in Fig. 4, the enhanced work functions kept more than half of the initial values for ten days, meaning that the changes induced by the treatment are quasi-stable.

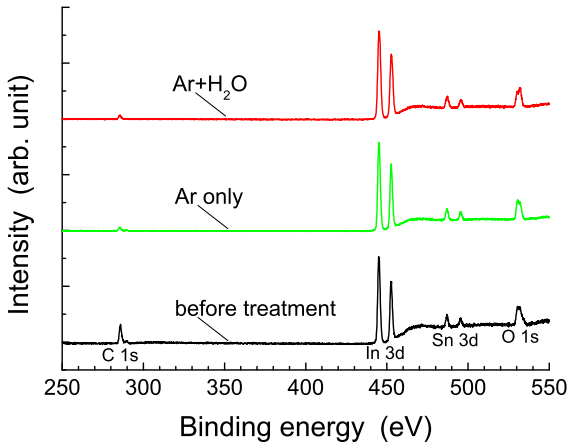

(a)

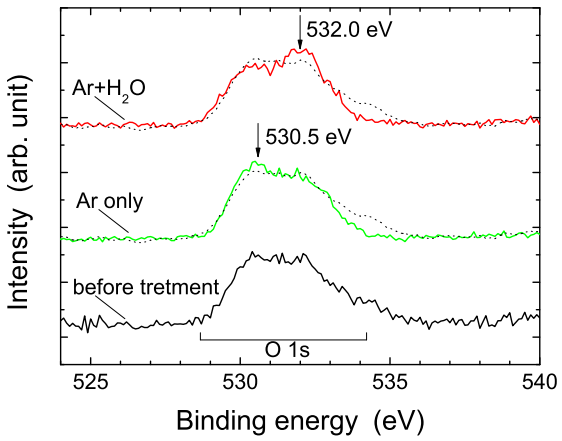

(b)

Fig. 6. (a) X-ray photoelectron spectra of films in various treatment cases of ITO surfaces. (b) Enlarged views of spectra around O 1s. Dotted lines indicate case before treatment shown in same figure for comparison.

3.2 Treatment of ITO electrode in OLEDs

We applied this method to the specific fabrication of electronic devices, treated the ITO electrode in the OLED by this method, and examined the OLED characteristics. Figure 7(a) shows the current density-voltage characteristics of the OLEDs fabricated in this experiment. In comparison with the no treatment case, the Ar plasma treatment

(without H_2O bubbling) significantly reduced the operation voltage to obtain a given current density exceeding 0.2 mA/cm^2. For comparison, we made a sample with similar process parameters except for the UV-O_3 treatment of the ITO,[17] which was already established in our fabrication line. Although it outperformed the Ar plasma treatment method, our scheme is quite promising since we had not optimized the parameters for the OLED fabrication processes. Furthermore, the Ar plasma treatment required only two minutes for this performance, which was much shorter than the UV-O_3 method's $\sim$ 30 minutes.

Figure 7(b) shows the external quantum efficiency for various current densities. At a given current density, the efficiency for the Ar plasma treatment showed maximum in all the cases. These results confirm that our proposed scheme has potential in the dry processes of some electronic devices to control the electronic states on solid surfaces.

3.3 Diagnostics of gaseous phases

To reveal the control mechanisms of surface electronic states in the downstream regions of atmospheric-pressure plasmas, we diagnosed gaseous phases in and just after the plasma generation region.

Figure 8 shows the spectra of the optical emissions from the atmospheric-pressure plasma regions. In our previous studies,[4] we measured electron density n_e in similar plasmas generated using fabric-type electrodes. n_e was in the order of 10^{12} cm^{-3}, which was higher than that in the conventional parallel-plate dielectric barrier discharges.[22] In another report,[5] we showed that the emission of OH($A^2\Sigma^+$), which is an excited state and emits light around 309 nm, was enhanced by water vapor introduction, although the ambient gases in that experiment were air. In contrast to that result,[5] in the experiments shown here, such air components as N_2 and O_2 were removed, and experiments were performed in a closed acrylic chamber.

Figure 8 also indicates that the main gas species for the discharges were Ar whose detectable emission spectra are distributed in a wavelength range exceeding 680 nm, and OH($A^2\Sigma^+$) was generated whose emission is observed around 309 nm. On the other hand, from N_2 we detected no signals, even though they are usually detected at 310-400 nm, and the OI emission at 777 nm from the excited atomic oxygens decomposed from O_2 was also under the detection limit. When we generated atmospheric O_2 plasma using a similar fabric-type electrode, we detected OI,[23] but this was not the case in our experiment. These results indicate that all the detectable gas species in the discharge

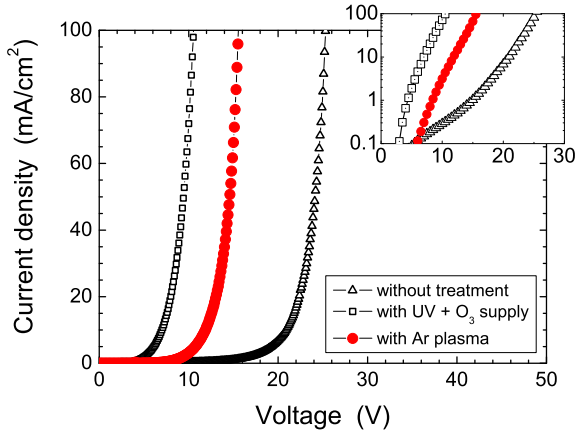

(a)

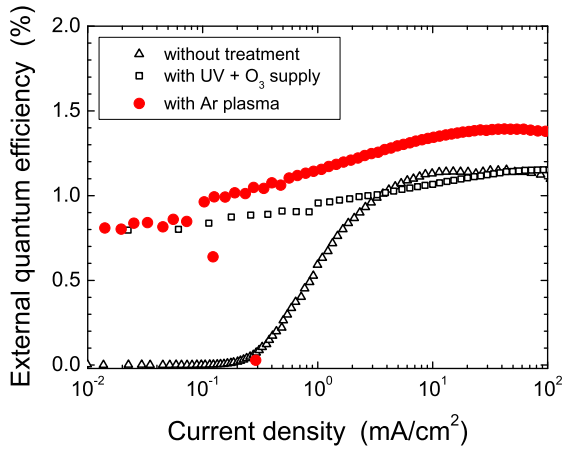

(b)

Fig. 7. (a) Current-voltage characteristics of organic light-emitting diodes (OLEDs) in various treatment schemes of ITO electrode surfaces. Inset is log plot of same data with same axes and units. (b) Quantum efficiencies of OLEDs similar to (a).

space are supplied from the Ar gas container and H_2O vapor.

From the optical emission spectra, we recognize the presence of corresponding gas species, but estimating their density is quite difficult. In our experimental apparatus, an available diagnostic method of the densities of key species is absorption spectroscopy in the ultraviolet ray region, in which O_3 has a sufficient absorption cross section.[24)]

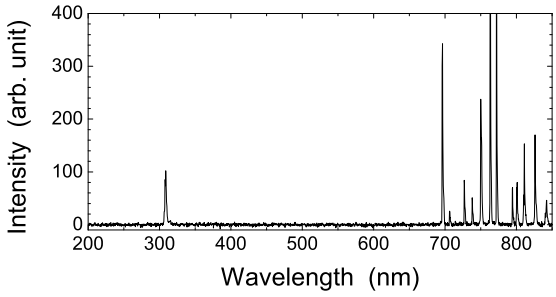

(a)

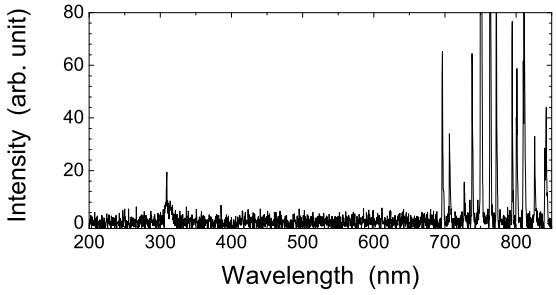

(b)

Fig. 8. Spectra of optical emissions from atmospheric-pressure plasma regions: (a) Ar plasmas without water vapor supply; (b) Ar plasmas with water vapor supply.

Figure 9 shows the absorption spectra of O_3. These measurements were performed in a teflon chamber with a smaller inner diameter (70 mm) to obtain an optical path around the electrode and the substrate, although the electrode and the gas-flow configuration were very similar to those in Fig. 1. The spectrum in the case of the Ar supply with water vapor indicates the generation of large density O_3, which was $\sim 3 \times 10^{15}$ cm^{-3} from Lambert-Beer's law and the absorption cross section of 1.147×10^{-17} cm^2.[24,25] However, the O_3 density in the case of the Ar supply without water vapor was rather small ($\sim 2 \times 10^{14}$ cm^{-3}).

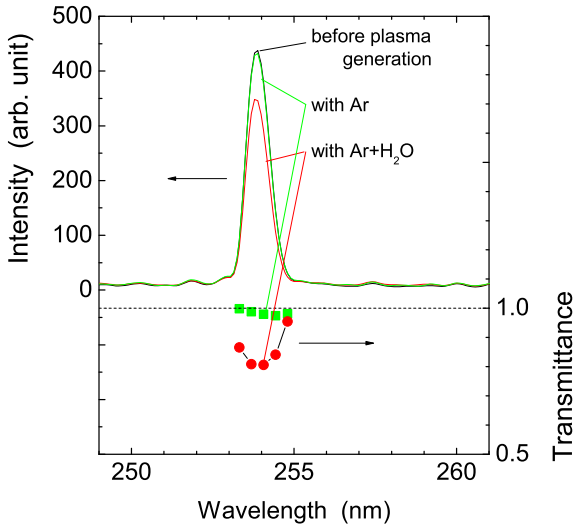

Fig. 9. Spectra of Hg lamp used for O_3 detection, and absorption spectra O_3 with and without water vapor

3.4 Discussion

Our experimental results on the control of the work function verify that its rapid and efficient increase is possible with this method. However, the underlying physics in the gaseous phase, in which some oxidants are transported from laminar atmospheric-pressure plasmas to the surfaces of metal oxides, is complicated and has not been clarified from the raw data shown in the experimental results (Figs. 8 and 9) on the diagnostics of the gaseous phases. Here, to point out the potential mechanisms, we analyze the facts shown in both figures and described in Subsection 2.2.3 with the extra information from the chemical reactions in the literature.

Because this treatment system is a remote-type configuration of atmospheric-pressure plasmas, O atoms cannot play direct and important roles. The candidates of the main oxidants are restricted to O_3 and OH(X), both of which have relatively longer lifetimes than O atoms at the atmospheric pressure. We detected the density of O_3 shown in Fig. 9. OH(X) is in the ground state, unlike OH($A^2\Sigma^+$), which was detected as emission at 309 nm (Fig. 8), and OH(X) density is usually much higher than OH($A^2\Sigma^+$). As shown in the previous report,[26] OH(X) radicals have densities around $10^{12} - 10^{15}$ cm^{-3} in atmospheric-pressure plasmas.

The optical emission spectra in Fig. 8 indicate that the density of O_2 is below the detection limit of the OES measurement. However, since OH($A^2\Sigma^+$) was certainly

observed, the H_2O introduced in the bubbling procedure should be adsorbed on the walls of the gas tubing system and the chamber; in general, Ref.[1)] indicates that molecules are very likely adsorbed on solid surfaces in physisorption states.

Another fact we have to pay attention to is the observation of higher density O_3 in the case with water vapor. The introduction of H_2O molecules may enhance the O_3 generation by the following sequential reactions in which OH(X) plays important roles,[26–28)] where k is the reaction rate constant, and M is other molecules, atoms, or surface whose area is large on fabric-type electrodes:

$$\mathrm{OH(X)} + \mathrm{OH(X)} \rightarrow \mathrm{H_2O} + \mathrm{O} \ \left(k = 1.42 \times 10^{-12}\,\mathrm{cm^3/s}\right), \tag{1}$$

$$\mathrm{OH(X)} + \mathrm{O} \rightarrow \mathrm{O_2} + \mathrm{H} \ \left(k = 3.33 \times 10^{-11}\,\mathrm{cm^3/s}\right), \tag{2}$$

$$\mathrm{O} + \mathrm{O_2} + \mathrm{M} \rightarrow \mathrm{O_3} + \mathrm{M} \ \left(k(300\mathrm{K}) = 6.09 \times 10^{-34}\,\mathrm{cm^6/s}\right), \tag{3}$$

In our previous report,[5)] we summarized the effects of the O_2 plasma treatment reported in Refs.[19,20)] and briefly review them in the following. The increase in the work function was attributed to an oxide-rich region induced on a very thin layer on the ITO surface by direct plasma treatment at low pressures and at atmospheric pressure. For instance, inductively coupled O_2 plasmas induced an oxide-rich region by the possible incorporation of O atoms on the surface, which leads to an increase in the work function. Atmospheric-pressure air plasmas also played an important role to create such oxidants as O and O_3 that contribute to the formation of an oxide-rich layer on the ITO surface and a resultant increase of the work function.

From our experimental results, the facts from previous studies, and suggestions from the literature, we summarize the following underlying physics that are specific in our method. For the case without water vapor:

(a1) H_2O and O_2, which are impurities (at low densities) that are adsorbed on the solid surfaces, are detached into the discharge space.

(a2) H_2O is decomposed partly into OH(X) by electron dissociation and partly into $OH(A^2\Sigma^+)$ by collisions with Ar and electrons (shown in Fig. 8). Some fraction of OH(X) becomes O_3 (indicated in Eqs. (1)-(3)).

(a3) O_2 mainly contributes to yield O_3. (O_3 from OH(X) and/or O_2 is shown in Fig. 9.)

(a4) Consequently, O_3 and OH(X) are the existing oxidants.

On the other hand, for the case with water vapor:

(b1) H_2O is supplied as one main discharge gas species. On the other hand, O_2, from the surface by detachment, is just an impurity species with much lower density.

(b2) Much H_2O is decomposed partly into OH(X) by electron dissociation and partly into OH($A^2\Sigma^+$) (shown in Fig. 8). Some fraction of OH(X) becomes O_3 (indicated in Eqs. (1)-(3)). The density of OH(X) is much higher than that in the case in (a2).

(b3) O_2 contributes to yield O_3, but the density of the generated O_3 from O_2 is lower than that from H_2O. (The total O_3 in shown in Fig. 9.)

(b4) Consequently, OH(X) is the major oxidant with much higher density, and O_3 is the minor one.

Note that plasmas with water vapor have smaller electron density than those without vapor,[14] which was partly indicated in weaker emissions in Fig. 8(b), and so the total densities of the oxidants may be in the same order in both cases with and without water vapor.

One report using low-pressure O plasma and Ar^+ irradiation[29] demonstrated that the OH group on ITO is less effective for the work function of ITO, which does not seem consistent with our results. Insertion of the OH group by Ar^+ irradiation and H_2O dose is shown in the same report,[29] which is one promising method. In our case, the ions in plasmas have almost no effect since the substrates were apart from the plasmas at the atmospheric pressure. Another different point in our study is the treatment in the surface equilibrium at the atmospheric pressure and a huge amount of such oxidants as O_3 and OH(X) that were supplied as gas flux. Even though such oxidants remove the C-oriented organic impurities for surface cleaning, they are on the ITO surfaces in equilibrium in physisorption and chemisorption, leading to rapid and stable change of the surface electronic states.

4. Concluding remarks

We examined the effects of atmospheric-pressure plasmas on the enhancement of work function on ITO and GZO surfaces. Using fabric-type electrodes, the work function of the ITO film installed in the downstream region of the plasma layer increased in a few minutes' treatment with good stability for several days. We confirmed enhancement

of the emission efficiency in OLEDs by this surface treatment of ITO electrodes and addressed the possible underlying mechanisms of oxidant generation and their spatial transport based on the diagnostics in the discharge and the downstream regions in our remote plasma configuration.

Acknowledgment

This work was partly supported by a Grant-in-Aid for Scientific Research from the Japanese Ministry of Education, Culture, Sports, Science and Technology.

References

1) A. Zangwill: *Physics at Surfaces* (Cambridge University Press, New York, 1988).
2) T. Matsushima and H. Murata: J. Appl. Phys. **104** (2008) 034507.
3) O. Sakai, Y. Kishimoto and K. Tachibana: J. Phys. D: Appl. Phys. **38** (2005) 431.
4) O. Sakai and K. Tachibana: J. Phys. Conf. Series **86** (2007) 012015.
5) O. Sakai, T. Morita, Y. Ueda, N. Sano, and K. Tachibana: Thin Solid Films **519** (2011) 6999.
6) K. Urabe, O. Sakai and K. Tachibana: J. Phys. D: Appl. Phys. **44** (2011) 115203.
7) Y. Ito, O. Sakai and K. Tachibana: Thin Solid Films **518** (2010) 3513.
8) K. Urabe, K. Yamada and O. Sakai: Jpn. J. Appl. Phys. **50** (2011) 116002.
9) S. -J. Park, K. S. Kim and J. G. Eden: Appl. Phys. Lett. **86** (2005) 221501.
10) O. Sakai, K. Tachibana, K. Tatsugawa, K. Ohishi and R. Inoue: Trans. Mater. Res. Soc. Jpn. **31** (2006) 453.
11) U. Kogelschatz: Contrib. Plasma Phys. **47** (2007) 80.
12) F. Iza, G. J. Kim, S. M. Lee, J. K. Lee, J. L. Walsh, Y. T. Zhang and M. G. Kong: Plasma Process. Polym. **5** (2008) 322.
13) D. Mariotti and R. M. Sankaran: J. Phys. D: Appl. Phys. **43** (2010) 323001.
14) Y. Ito, O. Sakai and K. Tachibana: Plasma Source Sci. Technol. **19** (2010) 025006.
15) N. A. Surplice and R. J. D'Arcy: J. Phys. E **3** (1970) 477.
16) Y. Gotoh, H. Tsuji and J. Ishikawa: J. Vac. Sci. Technol. B **21** (2003) 1607.
17) S. -Y. Kim, J. -L. Lee, K. -B. Kim and Y. -H. Tak: J. Appl. Phys. **95** (2004) 2560.
18) R. U. Olivares, T. Oda, Y. Oya, S. Tanaka and K. Tsuchiya: Fusion Eng. Des. **75-79** (2005) 765.
19) K.-H. Lee, H.-W. Jang, K.-B. Kim, Y.-H. Tak, J.-L. Lee: J. Appl. Phys. **95** (2004) 586.
20) J.-H. Choi, E.-S. Lee, S.-H. Choi, H.-K. Baik, K.-M. Song, Y.-S. Lim, S.-M. Lee: J. Vac. Sci. Technol. A **23** (2005) 1479.
21) T. Matsushima, G.-H. Jin, Y. Kanai, T. Yokota, S. Kitada, T. Kitada and H. Murata: Org. Electron. **12** (2011) 520.
22) K. Tachibana, Y. Kishimoto and O. Sakai: J. Appl. Phys. **97** (2005) 123301.
23) O. Sakai, M. Kimura, T. Shirafuji and K. Tachibana: Appl. Phys. Lett. **93** (2008) 231501.
24) D. C. Asthoitz, A. E. Croce and J. Troe: J. Phys. Chem. **86** (1982) 696.

25) S. O. Keeffe, C. Fitzpatrick and E. Lewis: Electron. Lett. **41** (2005) 1317.
26) C. Hibert, I. Garand, O. Motret and J. M. Pouvesle: J. Appl. Phys. **85** (1999) 7070.
27) R. Peyrous, P. Pignolet and B. Held: J. Phys. D: Appl. Phys. **22** (1989) 1658.
28) S. Pekarek and R. Balek: J. Phys. D: Appl. Phys. **37** (2004) 1214.
29) D. J. Milliron, I. G. Hill, C. Shen, A. Kahn and J. Schwartz: J. Appl. Phys. **87** (2000) 572.